Water Science & Technology

Water Science & Technology Vol 00 No 0, 1 doi: 10.2166/wst.2024.365

Phytomediated synthesis of WO_3 nanoparticles using *Solanum lycopersicum* fruit extract *for* enhanced photocatalytic activity of 2,4-dichlorophenol

S. Natchathra, G. Indramahalakshmi and Balasubramani Kavitha *

P.G and Research Department of Chemistry, C.P.A College, Bodinayakanur, Tamilnadu 625513, India
*Corresponding author. E-mail: kaviravee@gmail.com

BK, 0000-0002-4428-6528

ABSTRACT

In the present study, bio-citric acid/tungsten oxide (WO_3) (BCAWO) nanoparticles (NPs) were prepared by using *Solanum lycopersicum* fruit extract as a reducing as well as a capping agent. The photocatalysts were characterized by UV–vis diffuse reflection spectroscopy, powder X-ray diffraction (XRD), scanning electron microscopy (SEM), energy dispersive X-ray spectrometry (EDS), high-resolution transmission electron microscopy, and photoluminescence spectroscopy techniques. Diffraction peaks in the XRD spectrum were identified as the crystal planes of crystalline tungsten oxide. The BCAWO had an average size of 23.14 nm. For W–O bonds, the Fourier transform infrared spectrum displays the vibrational peak at 671.23 cm^{-1}. A prominent absorption band was observed at 268 nm, indicating the 1.2 eV bandgap. Under xenon (Xe) lamp irradiation, the synthesized BCAWO nanoparticles showed notable photocatalytic degradation of 2,4-dichlorophenol (2,4-DCP), with a degradation rate of 96%. With BCAWO concentrations of 2.5 g/L, pH of 4, reaction period of 180 min, and 2,4 DCP concentration of 10 mg/L, the degradation of 2,4-DCP had the highest efficacy, 96%. The degradation of phenols in wastewater may be facilitated by using the green WO_3 nanoparticles as a photocatalyst, according to the results.

Key words: 2, 4-dichlorophenol, citric acid, *Solanum lycopersicum*, tungsten oxide

HIGHLIGHTS

- Bio-citric acid/WO_3 (BCAWO) nanoparticles were prepared by using *Solanum lycopersicum* fruit extract as reducing as well as capping agents.
- The synthesized nanoparticles were characterized using UV–vis–diffuse reflection spectroscopy, Fourier transform infrared spectroscopy, X-ray diffraction, scanning electron microscopy, high-resolution transmission electron microscopy, and EDS.
- Efficient degradation of 2,4-dichlorophenol was achieved.
- The removal percentage of BCAWO could reach 96%.
- The reusability of our catalyst BCAWO was also studied.

GRAPHICAL ABSTRACT

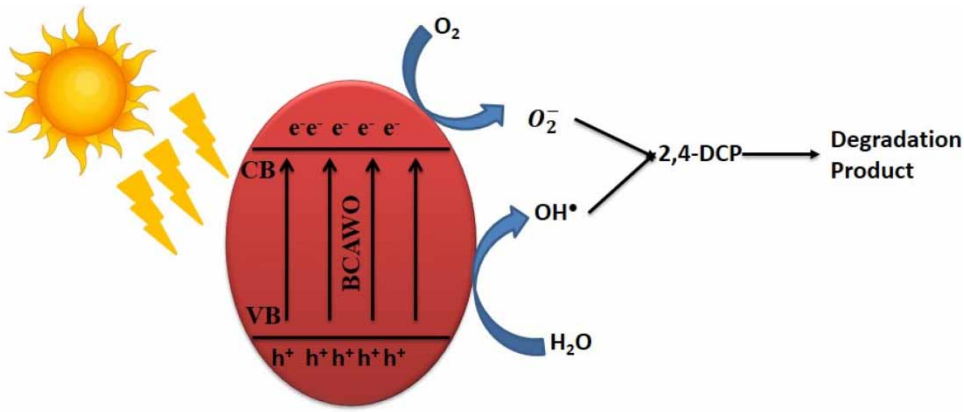

1. INTRODUCTION

It is increasingly recognized that the environmental implications of nanotechnologies should be understood better before further technological development takes place. The toxic organic chemicals discharged from various industrial processes and human activities contaminate the global water supply, which is a serious problem for living beings. Heterogeneous photocatalysis (one kind of advanced oxidation process (AOP)) has been considered a cost-effective alternative for the purification of dye-containing wastewater (Grzechulska & Morawski 2002; So *et al.* 2002). It has been proposed as a promising process to remove pollutants from air and water streams due to the possibility of organic pollutants' oxidation to CO_2 and H_2O in the presence of semiconductors (Su *et al.* 2012; Affam & Chaudhuri 2013; Cybula *et al.* 2014; Zhao *et al.* 2014; Saxena *et al.* 2016; Handojo *et al.* 2020; Hamza *et al.* 2023; Fatima *et al.* 2024; Shakoor *et al.* 2024; Tayyab *et al.* 2024). This process is very useful for removing highly toxic and hazardous organic pollutants that are miscible in water and difficult to remove through conventional methods.

Aromatic compounds are common pollutants in the waste effluent discharged by many factories and industry processes, including chemical plants, petroleum refineries, phenolic resins, caprolactam textile facilities, and some pharmaceutical processes (Li *et al.* 2009; Wang *et al.* 2009). Among the aromatic compounds, phenolic products are toxic to humans and aquatic organisms and are listed as one of the most common and serious environmental contaminants in water (Li *et al.* 2009). Due to the toxicity and consequent health hazards of phenolic compounds, these products have been placed on the list of priority pollutants by the US Environmental Protection Agency (Zhou *et al.* 2011). Chlorophenols are widely generated from a number of industrial manufacturing processes, such as pesticide, paint, solvent, pharmaceutical, wood-preserving chemicals, coke-oven, and pulp industries (Kilic & Cinar 2008). These compounds pose severe problems to the environment because they are carcinogens and mutagens. For example, 2,4-dichlorophenol (2,4-DCP) may cause some pathological symptoms and changes in human endocrine systems. Their mode of exposure is through the skin and the gastrointestinal system (Ranjit *et al.* 2008; Jia *et al.* 2012). They have been used extensively in many industrial products such as petrochemicals, pharmaceuticals, dyes, pulps, pesticides, and paints (Hameed *et al.* 2008; Zhang *et al.* 2010; Zhou *et al.* 2010; Ren *et al.* 2011; Chung *et al.* 2013); therefore, chlorophenols are common chloroaromatic pollutants (Olaniran & Igbinosa 2011). Removing these contaminants from water is a significant challenge because of ever-increasing pollution and the shortage of high-quality fresh water (Liu *et al.* 2012). The removal of these hazardous organic pollutants has become necessary and important for environmental safety.

Most of the methods used for the transformation of wastes and pollutants and treating wastewater are physical, chemical, or biological. Chemical transformations involve the application of reagents and reaction conditions to transform and treat target species. Moreover, recent studies have demonstrated that photocatalysis can be used to mineralize organic compounds or degrade dyes under UV irradiation. Tungsten oxide (WO_3), an important n-type semiconductor, has received wide attention owing to its promising application for electrochromic and photochromic devices, secondary batteries, and photocatalysts (Hong *et al.* 2009; Ghazal *et al.* 2022; Matalkeh *et al.* 2022). In addition, WO_3 possesses a small band gap energy falling within the solar spectrum (about 2.7–2.8 eV for WO_3), which implies that it has potential applications under visible light in the environmental field. However, the photocatalytic activity of WO_3 under visible light is limited due to the drawback that WO_3 has a conduction band (CB) edge lying in a position unfavourable for single-electron reduction of O_2, leading a poor photocatalyst for organic degradation under O_2 conditions. The photocatalytic and sensing applications of several types of WO_3 nanomaterials have been reported, which show great potential for human health, environmental protection and remediation, and energy conversion (Inoue *et al.* 1995; Bamwenda & Arakawa 2001). However, several fundamental issues must be addressed before they are economically viable for large-scale industrial applications. For example, pure WO_3 nanomaterials are usually not efficient photocatalysts because of the high electron–hole recombination rate and the difficulty in the reduction of oxygen. Owing to the high activation energy of reaction with gas molecules, the high work temperature and slow response time also restrict their gas sensing applications (Ozkan Zayim *et al.* 2003). Due to the wide range of applications, nanoparticles (NPs) of WO_3 have been synthesized by various experimental techniques, such as pyrolysis (Pokhrel *et al.* 2009), thermal decomposition (Zhao & Miyauchi 2008), sol–gel (Zheng *et al.* 2011), colloidal process (Sun *et al.* 2000), and ion-exchange methods (Lu *et al.* 2002).

Biogenic synthesis is useful not only because of its reduced environmental impact (Shankar *et al.* 2004; Anastas & Zimmerman 2007; Dahl *et al.* 2007) compared with some of the physicochemical production methods but also because it can be used to produce large quantities of nanoparticles that are free of contamination and have a well-defined size and morphology.

Biosynthetic routes can actually provide nanoparticles of a better-defined size and morphology than some of the physico-chemical methods of production. Compared with the use of whole plant extracts and plant tissue, the use of plant extracts for making nanoparticles is simpler. Plant extract–mediated synthesis is an increasing focus of attention. Processes for making nanoparticles using plant extracts are readily scalable and may be less expensive compared with the relatively expensive methods based on microbial processes. Plant extracts may act both as reducing agents and stabilizing agents in the synthesis of nanoparticles. The source of the plant extract is known to influence the characteristics of the nanoparticles. This is because different extracts contain different concentrations and combinations of organic reducing agents.

Tomatoes, or *Solanum lycopersicum*, are a healthy, nutrient-rich vegetable that have a broad range of anti-disease properties. The main ingredient in many meals is the tomato. The plant is native to South West America and is a member of the nightshade family, Solanaceae. Tomatoes include lycopene as well as a number of phenolic chemicals, flavonoids, and vitamins that have strong antioxidant properties. Plants are essential to the development of novel medications. As reducing agents, pro-oxidant metal complexes, free radical scavengers, and singlet oxygen production quenchers, antioxidants are crucial in the prevention of human diseases (Matei *et al.* 2021; Trombino *et al.* 2021). Therefore, *S. lycopersicum* has numerous highly reactive chemical functions that use reducing agents and stabilizing agents in the synthesis of nanoparticles.

However, to date there has been no report on the synthesis and photocatalytic behaviour of biosynthesis of citric acid (CA)–modified WO_3 nanoparticles using *S. lycopersicum fruit extract* for the degradation of 2,4-dichlorophenol. In this study, we explore the use of a conventionally produced composite material made of biosynthesis of WO_3 nanoparticles modified with CA using *S. lycopersicum for* degradation of a 2,4-DCP solution. We aim to determine the optimal amount of composite material and the most suitable method for realizing the most efficient and cost-effective water treatment process. Distinguished visible-light-driven photocatalytic properties for organic pollutant decomposition are observed for the doped WO_3 nanoparticles. The results will shed light on the approach to exploit the superior performance of the materials.

2. EXPERIMENTAL

2.1. Preparation of bio-citric acid/WO_3

S. lycopersicum fruit juice was extracted from fresh tomatoes and centrifuged for 10 min to separate the solid matter. The *S. lycopersicum* fruit extract was added into 50 mL of 0.3 M sodium tungstate dehydrate ($Na_2WO_4.2H_2O$) solution and continuously stirred. CA was added to the abovementioned solution dropwise. The stirring condition was maintained for 2 h until the colour of the solution changed from white to yellow. The solid precipitate obtained was purified by repeated centrifugation at 10,000 rpm for 10 min. It was then dried in an air hot oven at 80 °C overnight and thereafter calcined at 400 °C for 4 h in a muffle furnace. The final bio-CA/WO_3 product was coded as BCAWO and bare WO_3 was coded as WO.

2.2. Evaluation of photocatalytic activity

Photoactivity studies were performed at atmospheric pressure and room temperature (25 °C). In a typical experiment, the catalyst (2.5 g) was dispersed in a 2,4-DCP solution (300 mL) with initial concentration of 10 mg/L and neutral pH (pH 4) under magnetic stirring. Subsequently, 2,4-DCP photooxidation runs were performed using an immersion type photoreactor. The Haber photoreactor system was used in all experiments. The light intensity of the UV lamp used for degradation experiments was recorded using a UV–vis spectrophotometer. The photoreactor system had a magnetic stirrer, which was used to achieve uniform conditions in the reaction mixture. Before the UV light was turned on, the solution was stirred for 30 min to ensure good adsorption equilibrium between the catalyst and the solution. After irradiation for 180 min, the 2,4-DCP solution was filtered through a membrane filter (pore size 0.45 mm).

$$\text{Photodegradation } (\%) = \frac{C_0 - C}{C_0} \tag{1}$$

Here C_0 is the concentration of dye before irradiation and C is the concentration of dye after a certain irradiation time.

2.3. Characterization methods

The synthesized nanoparticles were characterized by the following methods. UV-vis diffuse reflection spectrum (UV-vis DRS) measurements were carried out in a JASCO V-550 double beam spectrophotometer with a PMT detector equipped with an integrating sphere assembly, using $BaSO_4$ as a reference sample. The powder X-ray diffraction patterns were measured in an

X-ray diffractometer (XPERT PRO X-ray) using Cu Kα irradiation at 25 °C. Structural assignments were made with reference to the JCPDS powder diffraction files. The surface morphology was examined using scanning electron microscopy (SEM-JSM 6701F- 6701) in both secondary and backscattered electron modes and the elemental analysis was also detected by an energy dispersive X-ray spectroscopy (EDS) attached to the SEM. The absorption spectra were obtained using a UV-Vis spectrophotometer (JASCO-V-530). The surface morphology was also analysed by transmission electron microscopy (TECNAI G2 model). The functional group was predicted by a JASCO-4200 Fourier transform infrared spectrometer (FT-IR).

3. RESULTS AND DISCUSSION

3.1. UV-vis diffuse reflectance spectra

Figure 1 represents the UV-vis diffuse reflectance spectra of BCAWO. The absorption peak exhibiting at 553 nm is in agreement with the earlier studies on WO_3 NPs (absorption peak at 545 nm), which confirmed the presence of WO_3 NPs.

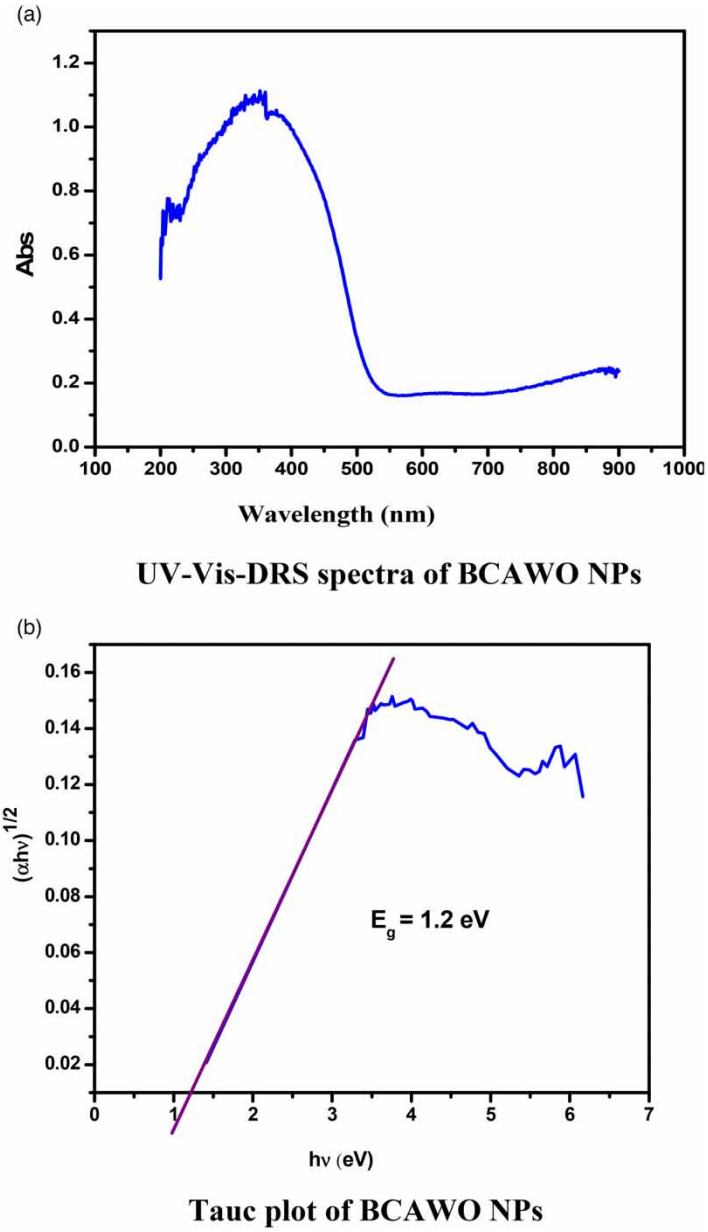

Figure 1 | (a) UV-vis DRS spectra of BCAWO NPs. (b) Tauc plot of BCAWO NPs.

Generally, the band gap energy of WO_3 is in the range of 2.6–3.0 eV, which corresponds to the excitonic wavelength range of 410–500 nm (Wang *et al.* 2013; Gan *et al.* 2016; Haryński *et al.* 2022; Kavitha *et al.* 2022). The band gap energy of a BCAWO can be calculated from the following formula:

$$(\alpha h\nu)^{1/n} = A(h\nu - E_g) \tag{2}$$

where h, ν, α, E_g, and A are the absorption coefficients, Planck's constant (6.626×10^{-34} J), light frequency, band gap energy, and a constant, respectively. The n is a factor that depends on the nature of the electron transition and is numerically equal to 1/2, 3/2, 2, or 3 for direct allowed, direct forbidden, indirect allowed, or indirect forbidden transitions, respectively. From Figure 1(b), E_g of WO_3 is estimated to be 1.2 eV according to a plot of $(\alpha h\nu)^{1/2}$ versus energy, which is red-shifted relative to the characteristic band gap energy of the bulk WO_3 ($E_g = 2.6$ eV) (Jubu *et al.* 2022).

3.2. Crystallographic analysis

Figure 2 represents the X-ray diffraction (XRD) patterns of BCAWO. The XRD pattern of green-CA/WO_3 shows that the synthesized NPs are highly crystalline and all the Bragg peaks can be indexed with the phase of WO_3 (JCDPS no. 410905), consistent with the selected area electron diffraction (SAED) result. The dominant peaks at $2\theta = 25.29$ and correspond to (100), (110), (111), (200), (210), and (211) diffraction peak of WO_3, respectively. The average crystalline size of the NPs as calculated by the Debye–Scherer equation is as follows:

$$D = \frac{0.9\lambda}{\beta\cos\theta} \tag{3}$$

where D is the crystallite size (diameter), λ is the wavelength of X-ray (1.54 Å), β is the value of full width at half height maximum of the most intense peak, and θ is Bragg's angle. The crystalline size of the BCAWO NPs was found to be around 23.14 nm.

3.3. Fourier-transform infrared spectrometer

FT-IR spectrometer is used to study the functional groups involved in the biosynthesis of green-CA/WO_3. The obtained FT-IR spectra of BCAWO exhibited prominent peaks at 362.62, 671.23, 933.55, and 1627.92 cm^{-1}. The FT-IR spectra record was

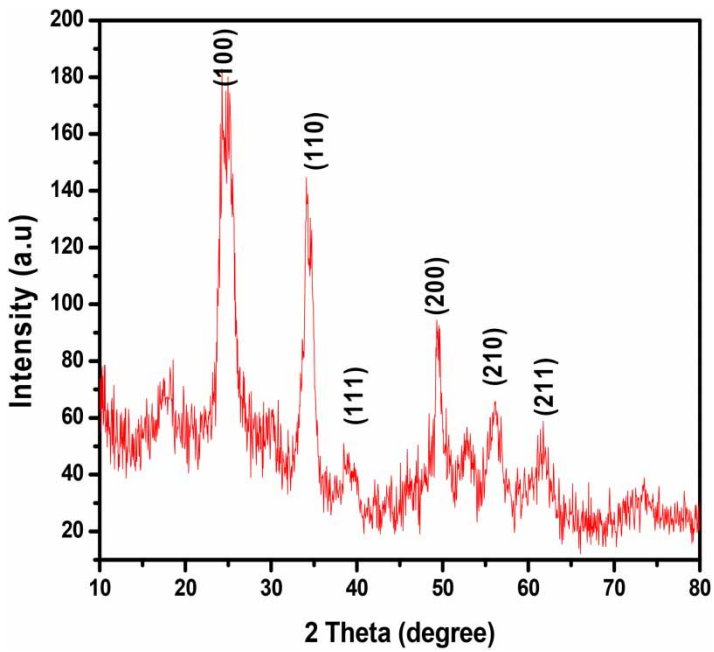

Figure 2 | XRD pattern of BCAWO NPs.

carried out in the range of 400–4,000 cm^{-1}. The existence of a bond at 671.23 cm^{-1} was recognized in the vibrations of W–O, confirming the formation of tungstate oxide nanoparticles (Guéry *et al.* 1997). In Figure 3, an intense band at 3,491 cm^{-1} proposes the presence of non-dissociated OH groups of CA. The peak around 2,918 cm^{-1} is due to CH_2 stretching, and the peak at 1,653 cm^{-1} may be assigned to the symmetric stretching of OH from the COOH group, displaying the binding of a CA radical to the WO_3 surface.

3.4. SEM, HRTEM, and EDS

The typical SEM and high-resolution transmission electron microscopy (HRTEM) images of BCAWO NPs are depicted in Figure 4(a) and 4(b). The SEM images showed that BCAWO NPs are polydispersed and roughly spherical in shape and pores. The EDS spectrum of BCAWO is shown in Figure 5. EDS analysis confirmed the presence of W, O, and C in the BCAWO. The presence of carbon, oxygen, and W indicated that the organic moieties are adsorbed on the surface of the WO_3 NPs.

The HRTEM image of BCAWO suggested that the sample has a well-defined crystalline structure, which is crucial for excellent photocatalytic activity. The images clearly show the presence of secondary material capping with a thickness of nm, which may be assigned to bioorganic compounds present in the fruit extract. Figure 4(c) shows the SAED pattern of BCAWO, which reveals the polycrystallinity of the prepared sample.

3.5. Photocatalytic activity

The photocatalytic activity of the BCAWO was tested using the decomposition of 2,4-DCP under visible light irradiation. Figure 6(a) shows the photocatalytic degradation of 2,4-DCP by BCAWO under visible light irradiation. A decrease of 2,4-DCP intensity at wavelength 442 nm is observed. Figure 6(b) shows the photocatalytic degradation of 2,4-DCP with BCAWO (96%, 75%) and without BCAWO (5%).

3.6. Kinetics

Generally, the photodegradation reaction of 2,4-DCP can be described by the Langmuir–Hinshelwood model when the concentration of the 2,4-DCP is in the millimolar range. To quantitatively investigate the reaction kinetics of the 2,4-DCP degradation, the experimental data were fitted by a first-order model as expressed by the following formula:

$$-\frac{dC}{dt} = kC \tag{4}$$

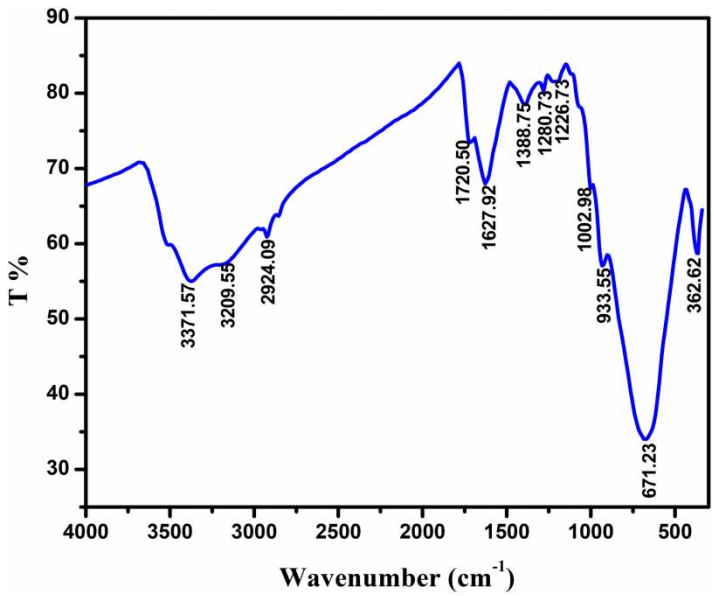

Figure 3 | FT-IR spectrum of BCAWO NPs.

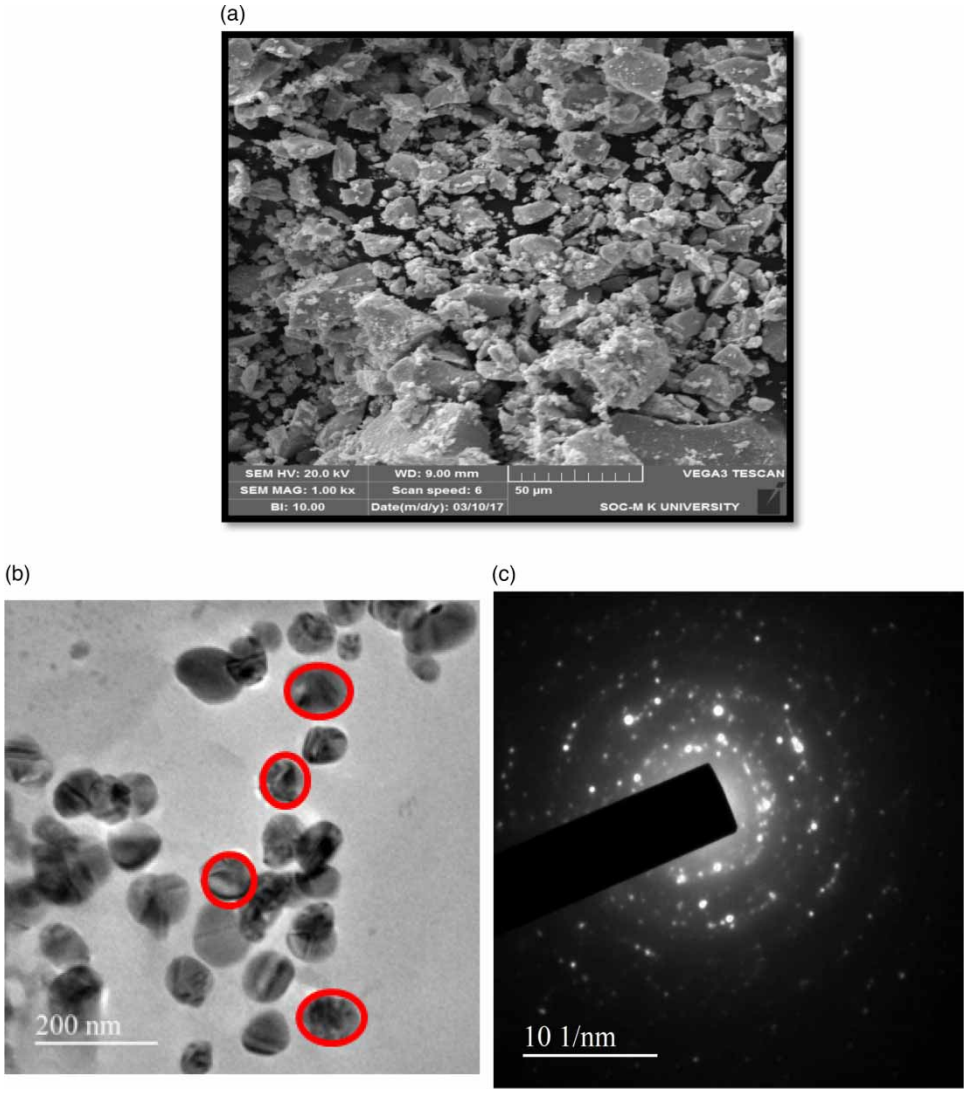

Figure 4 | (a) SEM image of BCAWO NPs. (b) HRTEM image of BCAWO NPs. (c) SAED pattern of BCAWO NPs.

where the initial condition of $C = C_0$ when $t = 0$. Then the equation becomes

$$-\ln\left(\frac{C}{C_0}\right) = kt \tag{5}$$

where C_0 and C are the 2,4-DCP concentrations in solution at times (t), respectively, and k is the apparent first-order rate constant. Upon varying the BCAWO content, the plot of the irradiation time (t) against $\ln(C/C_0)$ was nearly a straight line given in Figure 6(c). The rate constants are found to be 3.6×10^{-3}, 8.16×10^{-3}, and 2.02×10^{-2} for dark, without catalyst, and BCAWO, respectively. The activity of catalysts for the photodegradation of 2,4-DCP was studied with an initial concentration of 10 mg/L, catalyst dose of 2.5 g, and irradiation time of 180 min (Figure 6(c)).

3.7. Effect of pH

The pH of a solution is one of the most important parameters involved in the degradation of aqueous solution of 2,4-DCP (Kamaraj *et al.* 2022; Kamaraj & Balasubramani 2024). The effect of pH on the photodegradation of 2,4-DCP in the presence of BCAWO was investigated over a pH range of 3.0–10.0. The influence of initial pH generally depends on the type of compound that has to be degraded and the zero point charge (zpc) of the photocatalyst used in the oxidation process. The pH of

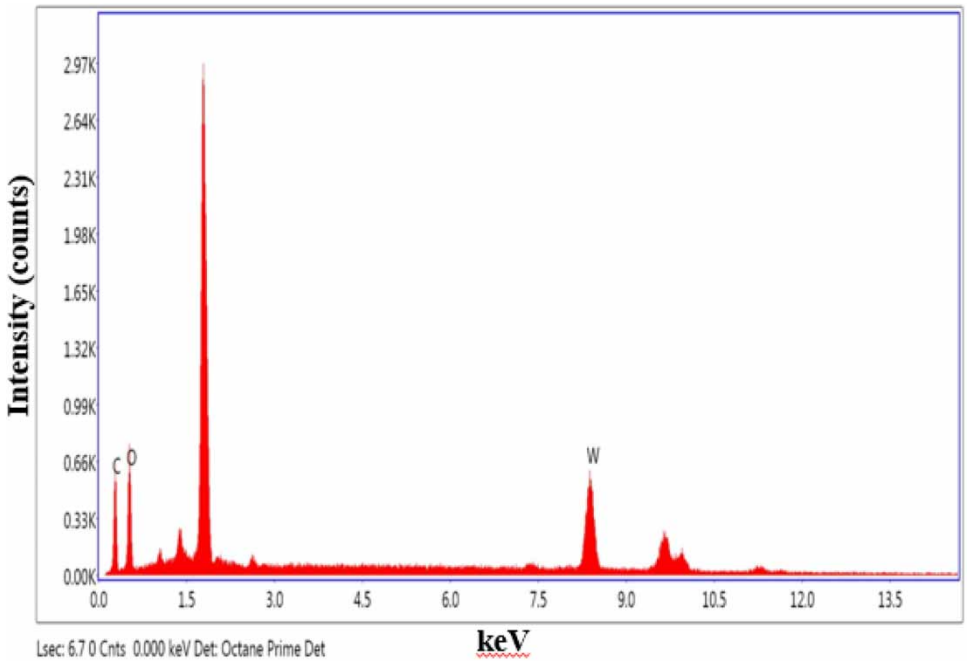

Figure 5 | EDS spectrum of BCAWO NPs.

the solution influences the surface charge properties of the photocatalyst and increases the electrostatic interaction between the nanocatalyst surface and the organic pollutant molecules. Figure 7(a) illustrates the effect of pH on the initial rate of photocatalytic degradation of phenol in the presence of the BCAWO nanocatalyst. In the presence of nano-BCAWO, the initial percentage degradation of 2,4-DCP was found to decrease with the increase in pH. Under mild acidic and neutral pHs, the percentage degradation was found to be almost the same (15–18%). At higher pH values, 2,4-DCP exists as a negatively charged phenolate species. Therefore, the adsorption of 2,4-DCP on the catalyst surface decreases. However, at pH 10.0, a slight increase in the degradation rate is observed, which may be due to the higher concentration of the hydroxyl ions. Therefore, 2,4-DCP degradation is more favourable in mild, acidic, and neutral pH on the surface of BCAWO. With nano-WO_3, a very high percentage degradation of 2,4-DCP was observed at lower pHs between 3.0 and 5.0, as shown in Figure 7(a). This increased degradation of 2,4-DCP can be attributed to the fact that WO is amphoteric in aqueous solution. The point of zero charge (pHpzc) of WO is 6.8. Below this value, the WO surface is positively charged and above it, it is negatively charged and results in high adsorption of 2,4-DCP on the catalyst surface.

3.8. Effect of catalyst dosage

Five different adsorbent dosages (0.5, 1, 1.5, 2, and 2.5 g) were studied for the removal of 2,4-DCP at a fixed initial concentration of 100 mg/L. Adsorbent dosage plays a significant role in the percentage of 2,4-DCP removal. It was clearly evident from the results that a gradual increase in the adsorbent dose leads to high percentages of 2,4-DCP removal. For each type of adsorbent, an adsorbent dose of 2.5 g showed the highest 2,4-DCP removal capacity, whereas 2,4-DCP removal efficiency was negligible for 0.5 g adsorbent dose. This may be due to increased adsorbent surface area and the availability of more adsorption sites resulting from the increased adsorbent dosage. This factor contributes to greater efficiency of 2,4-DCP removal. So, removal efficiency increases up to the optimum dosage beyond which removal efficiency decreases. This indicates that 2,4-DCP removal was effective in the dose ranges studied. The observed effect of catalyst loading on phenol degradation by solar photocatalysis is that although the number of active sites in solution increases with catalyst loading, a point appears to be reached where light penetration is compromised because of excessive particle concentration, resulting in optimum catalyst loading at which the degradation is the maximum.

3.9. Effect of initial 2,4-DCPconcentration

Successful application of the photocatalytic oxidation system requires the investigation of the dependence of the photocatalytic degradation rate on the substrate concentration. The effect of initial 2,4-DCP concentration on photocatalytic

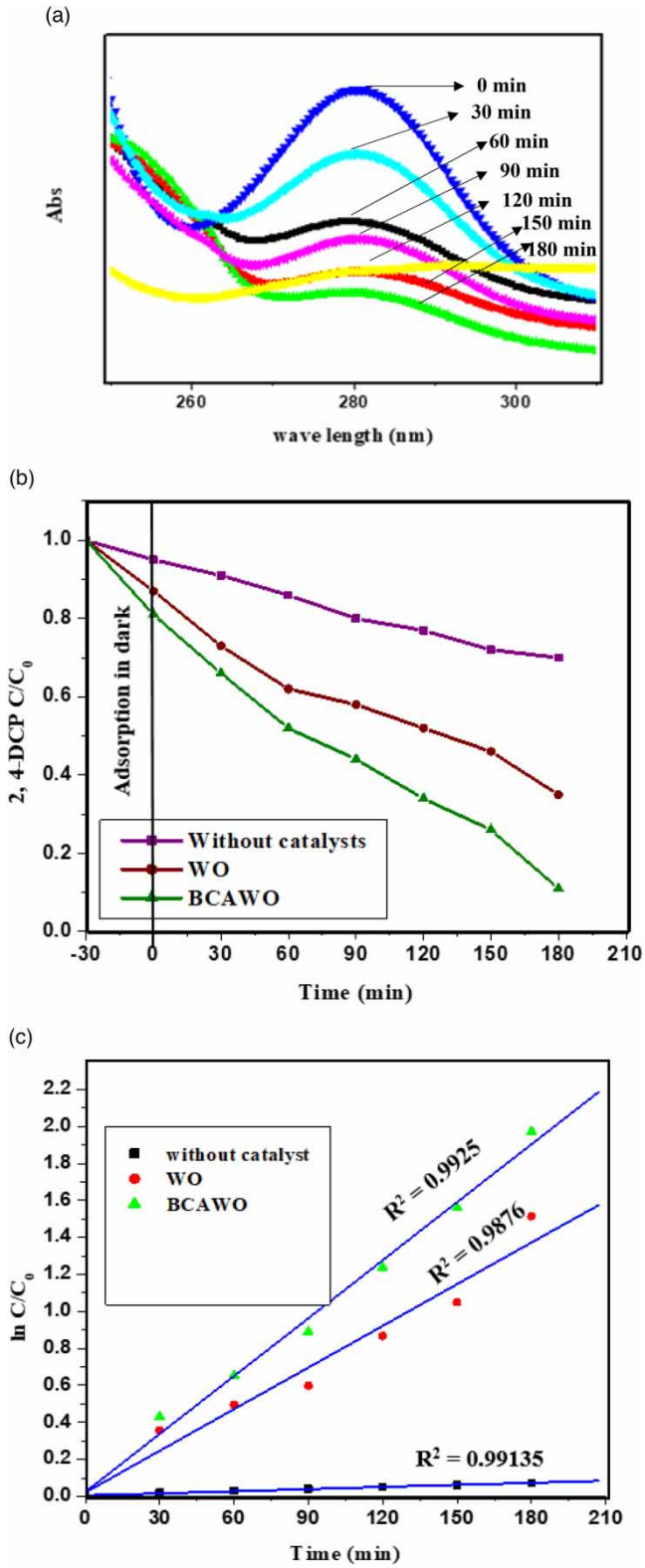

Figure 6 | (a) Time-dependent UV-vis spectral changes of 2,4-DCP in the presence of BCAWO under solar light irradiation. (b) Photodegradation of 2,4-DCP with BCAWO, WO, and without catalysts. (c). The kinetic plot of $-\ln(C/C_0)$ versus irradiation time for the photodegradation of 2,4-DCP using BCAWO NPs.

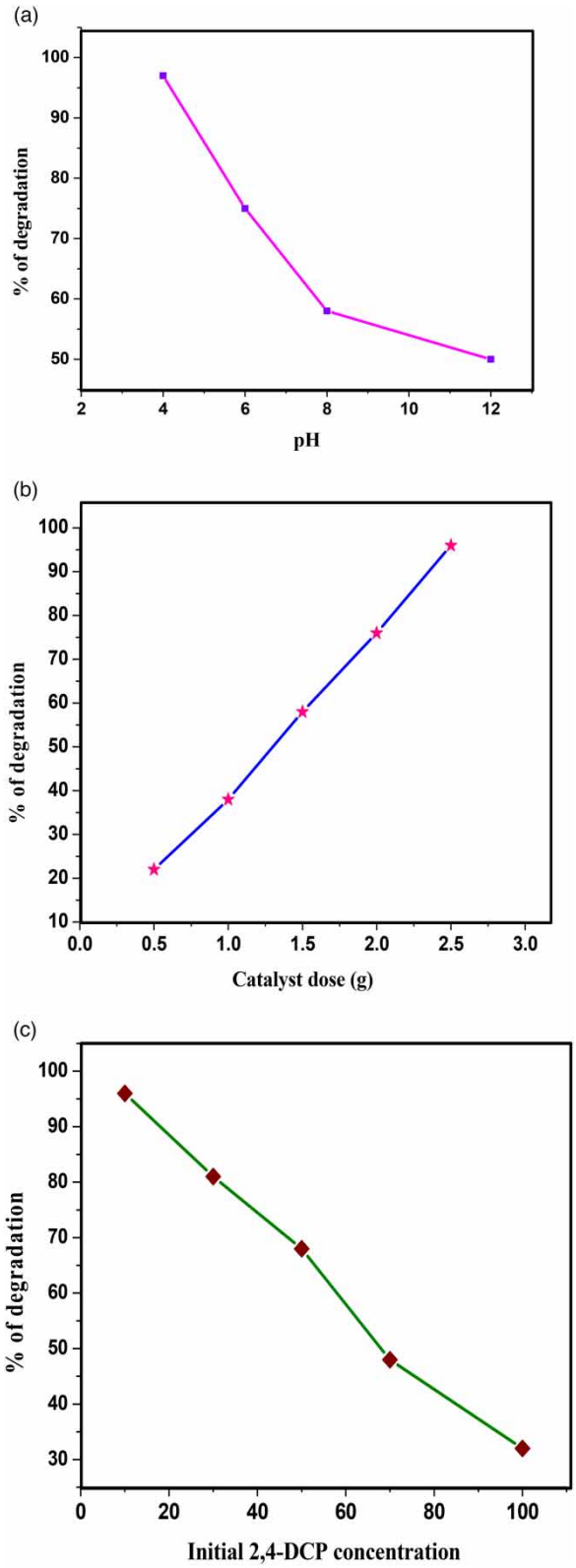

Figure 7 | (a) Effect of pH on degradation of 2,4-DCP using BCAWO NPs. (b) Effect of catalyst dose on degradation of 2,4-DCP using BCAWO NPs. (c) Effect of initial 2,4-DCP concentration on degradation of 2,4-DCP using BCAWO NPs.

degradation of phenol was studied with different initial 2,4-DCP concentrations of 10, 30, 50, 70, and 100 mg/L with initial pH of 4 and with BCAWO loading of 2.5 g/L. Figure 7(c) shows that the percentage degradation of 2,4-DCP decreased with increase in initial concentration of 2,4-DCP. With the fixed catalyst loading, when the initial phenol concentration increases, since the generation of OH^- does not increase, the probability of 2,4-DCP molecules to react with ^-OH decreases, therefore, the rate of 2,4-DCP degradation decreases. With 100 mg/L initial 2,4-DCP concentration, the degradation did not initiate for the first few min, showing the delay in photocatalysis. The delay may be owing to the generation of reactive hydroxyl radicals. At a higher initial 2,4-DCP concentration, the 2,4-DCP molecules present in the solution are higher leading to a higher number of collisions between the 2,4-DCP molecules themselves and thus the molecules compete for active sites. This competitive effect may lead to the displacement of 2,4-DCP molecules nearer to the catalyst surface by other colliding 2,4-DCP molecules, thus giving less time for them to adsorb on the surface active sites. Such a phenomenon would have resulted in delayed initiation of photocatalysis at high initial 2,4-DCP concentrations.

3.10. Mechanism

Figure 8 illustrates the photocatalytic process conducted on semiconductor materials. Semiconductors possess a band structure where the CB is separated from the valence band (VB) by a gap. Here, a simplified mechanism of BCAWO for the degradation of 2,4-DCP is proposed. In this scenario, electron–hole pairs are generated in the VB of BCAWO under sunlight. When the energy from sunlight exceeds the material's band gap, the generated electron is transferred to the CB of BCAWO, thereby creating holes in the valence band. The oxidation–reduction reaction occurs through the electron–hole pair, with the hole acting as an oxidant and the electron as a reductant. The electron–hole pairs produce superoxide anions (O_2^-) and hydroxyl radicals (OH^-). These species attack 2,4-DCP, leading to the dissociation into harmless products as the final degradation products. Thus, it is observed that CA, biomolecules, and their conjugation with WO_3 nanoparticles play a major role in enhancing the photocatalytic degradation of 2,4-DCP. The photocatalytic mechanism is as follows (Hu *et al.* 2018; Bayahia 2022):

$$\text{BCAWO} + h\nu \rightarrow \text{BCAWO}(h^+ + e^-)$$

$$\text{BCAWO}(h^+) + H_2O \rightarrow \text{BCAWO}(h^+) + OH^\bullet + H^+$$

$$\text{BCAWO} + O_2 + e^- \rightarrow \text{BCAWO} + O_2^-$$

$$OH^\bullet + O_2^- + 2,4\text{-DCP} \rightarrow \text{Degradation products}$$

3.11. Separation and reuse of photocatalysts

An attractive feature of photocatalytic materials is that the inherent structure of the catalyst is stable towards oxidative decomposition and that the photocatalyst can be facilely separated from the dispersion by simple centrifugation after reaction, which facilitates the reuse of the catalyst. In addition, as mentioned previously, the release of degraded intermediates

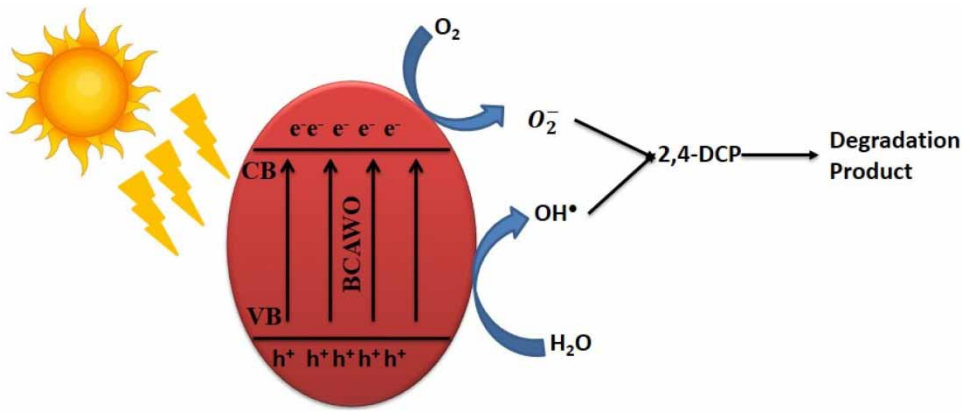

Figure 8 | Schematic energy level diagram of BCAWO NPs for the photocatalytic degradation of 2,4-DCP.

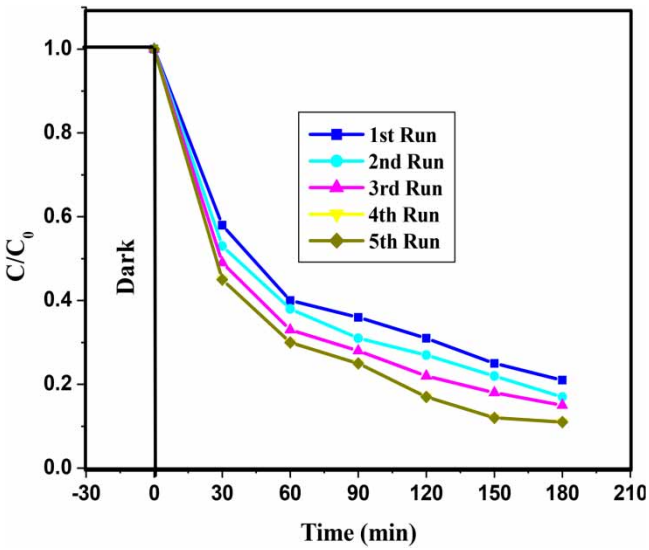

Figure 9 | Reusability of BCAWO NPs for degradation of 2,4-DCP.

from the catalyst surface can also prevent the catalyst surface from blocking and poisoning by the intermediates. In our experiments, the stability and reusability of the BCAWO were examined by repetitive use of the catalyst. The solution resulting from the photocatalytic degradation of 2,4-DCP was filtered and washed, and the photocatalyst was dried. The dried catalyst samples were used for the degradation of 2,4-DCP, employing similar experimental conditions. Under the present investigation, it was observed that the dissolution of the catalyst was found to be negligible. Catalyst samples showed considerably reproducible photocatalysis activity up to five cycles for the degradation of 2,4-DCP.

3.12. Chemical oxygen demand

The chemical oxygen demand (COD) is commonly used as an effective technique to assess the degree of mineralization reached during the photocatalytic treatment (Vignesh *et al.* 2012). The COD was determined by the standard dichromate method and the results are given in Table 1. To confirm the mineralization of 2,4-DCP, the degradation was analysed by COD values. The photocatalytic degradation experiments were performed under optimum conditions. Test samples were collected every 30 min during the process. The results indicated that, during the photodegradation process, most of the organic matter degrades to smaller species (especially inorganic compounds) and hence the required COD decreases. The percentage removal efficiency was calculated by the following formula:

$$\%\ \text{of COD removal} = \frac{[\text{COD}_{\text{blank}} - \text{COD}_{\text{CV}}]}{\text{COD}_{\text{blank}}} \times 100 \tag{5}$$

Table 1 | COD removal efficiency of 2,4-DCP

Time (min)	COD removal efficiency (%) 2,4-DCP
0	0
30	5.55
60	28.65
90	48.42
120	59.22
150	72.87
180	88.11

Table 2 | Comparison of degradation efficiency of various catalysts for 2,4-DCP

Catalyst name	Pollutant	Time	% degradation	Light source	References
Ag/AgX	2,4-DCP	300 min	83.37% 89.39%	UV Visible light	Moja *et al.* (2024)
TiO_2–CeO_2	2,4-DCP	360 min	49	Visible light	Gnanasekaran *et al.* (2021)
TiO_2 modified ZnO/SnO_2	2,4-DCP BPA	180 min	72% 58%	UV light	Ali *et al.* (2020)
ZnO–ZrO_2	2,4-DCP	300 min	90%	UV light	Sherlya *et al.* (2014)
Porphyrin/TiO_2	2,4-DCP	360 min	81%	Visible light	Nezamzadeh-Ejhieh & Ghanbari-Mobarakeh (2015)
Co/TiO_2	2,4-DCP	120 min	68.03%	Visible light	Hoseini *et al.* (2017)
Bio-CA/WO_3	2,4-DCP	180 min	96%	Visible light	Present work

3.13. Comparison of degradation efficiency

The literature (Sherlya *et al.* 2014; Nezamzadeh-Ejhieh & Ghanbari-Mobarakeh 2015; Hoseini *et al.* 2017; Ali *et al.* 2020; Gnanasekaran *et al.* 2021; Moja *et al.* 2024) presents photodegradation studies utilizing various photocatalysts for the removal of 2,4-DCP in aqueous solutions. Table 2 summarizes the findings of this comparison with previously published reports. When compared to earlier studies (Table 2), it can be concluded that the time needed for maximum removal of 2,4-DCP was shorter, at 180 min.

4. CONCLUSION

Improvement of these simple techniques to utilize solar radiation more efficiently could provide more economic solutions for the degradation of organic compounds such as 2, 4-DCP from water. However, due to the periodic availability of this source of energy, it cannot be used for continuous treatment of wastewater. Under such conditions, solar energy may be used during daytime and non-monsoon periods. Another alternative is to store wastewater generated during the night and treat it during daytime using a fluidized bed reactor operated in batch with recycle mode, so as to handle large quantities of wastewater. Thus, the BCAWO nanoparticles can be effectively used for the treatment of 2,4-DCP-contaminated water by solar photocatalysis. It is also evident that the reaction takes place via the formation of singlet oxygen, superoxide, and hydroxyl radicals. This methodology has an additional advantage of using the visible light of solar energy for the degradation of organic pollutants in water. Further studies to apply this synergistic technique using solar energy are underway.

DATA AVAILABILITY STATEMENT

All relevant data are included in the paper or its Supplementary Information.

CONFLICT OF INTEREST

The authors declare there is no conflict.

REFERENCES

Affam, A. C. & Chaudhuri, M. (2013) Degradation of pesticides chlorpyrifos, cypermethrin and chlorothalonil in aqueous solution by TiO_2 photocatalysis, *J. Environ. Manage.*, **130**, 160–165.

Ali, W., Ullah, H., Zada, A., Muhammad, W., Ali, S., Shaheen, S., Alamgir, M. K., Ansare, M. Z., Khanf, Z. U., Bilal, H. & Yap, P. S. (2020) Synthesis of TiO_2 modified self-assembled honeycomb ZnO/SnO_2 nanocomposites for exceptional photocatalytic degradation of 2,4-dichlorophenol and bisphenol A, *Sci. Total Environ.*, **746**, 141291.

Anastas, P. T. & Zimmerman, J. B. (2007) Green nanotechnology. In: *Why we Need A Green Nano Award and how to Make it Happen*, Washington, DC: Woodrow Wilson International Center for Scholars.

Bamwenda, G. R. & Arakawa, H. (2001) The visible light induced photocatalytic activity of tungsten trioxide powders, *Appl. Catal. A*, **210**, 181–191.

Bayahia, H. (2022) Green synthesis of activated carbon doped tungsten trioxide photocatalysts using leaf of basil (*Ocimum basilicum*) for photocatalytic degradation of methylene blue under sunlight, *J. Saudi Chem. Soc.*, **26**, 101432.

Chung, S. G., Chang, Y. S., Choi, J. W., Baek, K. Y., Hong, S. W., Yun, S. T. & Lee, S. H. (2013) Photocatalytic degradation of chlorophenols using star block copolymers: removal efficiency, by-products and toxicity of catalyst, *Chem. Eng. J.*, **215**, 921–928.

Cybula, A., Nowaczyk, G., Jarek, M. & Zaleska, A. (2014) Preparation and characterization of Au/Pd modified-TiO_2 photocatalysts for phenol and toluene degradation under visible light – The effect of calcination temperature, *J. Nanomate..*, **2014**, 1–9.

Dahl, J. A., Maddux, B. L. S. & Hutchison, J. E. (2007) Toward greener nanosynthesis, *Chem. Rev.*, **107**, 2228–2269.

Fatima, U., Rafique, H., Akram, S., Chen, S., Naseem, K., Najeeb, J. & Tayyab, M. (2024) Facile green synthesis of *Phyllanthus emblica* extract based Ag-NPs for antimicrobial and response surface methodology based catalytic reduction applications, *J. Cleaner Prod.*, **434**, 140003.

Gan, L., Xu, L., Shang, S., Zhou, X. & Meng, L. (2016) Visible light induced methylene blue dye degradation photo-catalyzed by WO_3/grapheme nanocomposites and the mechanism, *Ceram. Int.*, **42**, 15235–15241.

Ghazal, S., Mirzaee, M. & Darroudi, M. (2022) Green synthesis of tungsten oxide (WO_3) nanosheets and investigation of their photocatalytic and cytotoxicity effects, *Micro & Nano Lett.*, **17** (11), 286–298.

Gnanasekaran, L., Rajendran, S., Priya, A. K., Durgalakshmi, D., Vo, D.-V. N., Cornejo-Ponce, L., Gracia, F. & Soto-Moscoso, M. (2021) Photocatalytic degradation of 2,4-dichlorophenol using bio-green assisted TiO_2–CeO_2 nanocomposite system, *Environ. Res.*, **195**, 110852.

Grzechulska, J. & Morawski, A. W. (2002) Photocatalytic decomposition of azo-dye acid black 1 in water over modified titanium dioxide, *Appl. Catal. B: Environ.*, **36**, 45–51.

Guéry, C., Choquet, C., Dujeancourt, F., Tarascon, J. M. & Lassègues, J. C. (1997) Infrared and X-ray studies of hydrogen intercalation in different tungsten trioxides and tungsten trioxide hydrates, *J. Solid State Electrochem.*, **1**, 199–207.

Hameed, B. H., Tan, I. A. W. & Ahmad, A. L. (2008) Adsorption isotherm, kinetic modeling and mechanism of 2,4,6-trichlorophenol on coconut husk based activated carbon, *Chem. Eng. J.*, **144**, 235–244.

Hamza, M., Altaf, A. A., Kausar, S., Murtaza, S., Shahpal, A., Hamayun, M., Tayyab, M., Rizwan, K., Shoukat, H. & Maqsood, A. (2023) Mesoporous Cu-doped manganese oxide nano straws for photocatalytic degradation of hazardous alizarin red dye, *ACS Omega*, **8**, 35956–35963.

Handojo, L., Pramudita, D., Mangindaan, D. & Indarto, A., (2020) Application of nanoparticles in environmental cleanup: Production, potential risks and solutions. In: Bharagava, R. (ed.) *Emerging Eco-Friendly Green Technologies for Wastewater Treatment. Microorganisms for Sustainability*, Singapore: Springer, pp. 18. https://doi.org/10.1007/978-981-15-1390-9_3.

Haryński, L., Olejnik, A., Grochowska, K. & Siuzdak, K. (2022) A facile method for tauc exponent and corresponding electronic transitions determination in semiconductors directly from UV–vis spectroscopy data, *Opt. Mater.*, **127** (112205).

Hong, S. J., Jun, H., Borse, P. H. & Lee, J. S. (2009) Side effects of WO_3 nanocrystals for photooxidation of water in particulate suspension and photoelectrochemical film system, *Int. J. Hydrogen Energy*, **34**, 3234–3242.

Hoseini, S. N., Pirzaman, A. K., Aroon, M. A. & Pirbazari, A. E. (2017) Photocatalytic degradation of 2,4-dichlorophenol by Co-doped TiO_2(Co/TiO_2) nanoparticles and Co/TiO_2 containing mixed matrix membranes, *J. Water Process Eng.*, **17**, 124–134.

Hu, K., Li, Z., Chen, S., Bian, J., Qu, Y., Tang, J. & Jing, L. (2018) Synthesis of silicate-bridged heterojunctional sno$_2$/$BiVO_4$ nanoplates as efficient photocatalysts to convert CO_2 and degrade 2,4-dichlorophenol, *Part. Part. Syst. Charact.*, **35** (1700320).

Inoue, T., Ohtsuka, K., Yoshida, Y., Matsuura, Y. & Kajiyama, Y. (1995) Metal oxide semiconductor NO_2 sensor, *Sens. Actuators B.*, **24**, 388–391.

Jia, J., Zhang, S., Wang, P. & Wang, H. (2012) 'Degradation of high concentration 2,4-dichlorophenol by simultaneous photocatalytic–enzymatic process using TiO_2/UV and laccase', *J. Hazard. Mater.*, **29**, 150–155.

Jubu, P. R., Obaseki, O. S., Nathan-Abutu, A., Yam, F. K., Yusof, Y. & Ochang, M. B. (2022) Dispensability of the conventional tauc's plot for accurate bandgap determination from UV–vis optical diffuse reflectance data, *Results Opt.*, **9**, 100273.

Kamaraj, E. & Balasubramani, K. (2024) Development of a novel $CuWO_4$/SnO_2 heterogenous photocatalyst for effective rose bengal dye degradation under visible light, *Iran. J. Mater. Sci. Eng.*, **21** (2), 1–13.

Kamaraj, E., Lee, Y. R. & Balasubramani, K. (2022) Fabrication of a visible-light-driven p-type $NiWO_4$/n-type SnO_2 heterojunction with efficient photocatalytic activity for degradation of amaranth, *J. Chin. Chem. Soc.*, **1**.

Kavitha, B., Deepa, R. & Sivakumar, S. (2022) Evolvulus alsinoides plant mediated synthesis of Ag_2O nanoparticles for the removal of Cr(VI) ions from aqueous solution: modeling of experimental data using artificial neural network, *Mater. Today Sustain.*, **18**, 100124.

Kilic, M. & Cinar, Z. (2008) Hydroxyl radical reactions with 4-chlorophenol as a model for heterogeneous photocatalysis, *J. Mol. Struct.*, **851**, 263.

Li, M., Feng, C., Hu, W., Zhang, Z. & Sugiura, N. (2009) Electrochemical degradation of phenol using electrodes of Ti/$RuO_{(2)}$-Pt and Ti/$IrO_{(2)}$-Pt, *J. Hazard. Mater.*, **162**, 455–462.

Liu, L., Chen, F., Yang, F., Chen, Y. & Crittenden, J. (2012) Photocatalytic degradation of 2,4-dichlorophenol using nano scale Fe/TiO_2, *Chem. Eng. J.*, **181**, 189–195.

Lu, Z., Kanan, S. M. & Tripp, C. P. (2002) Synthesis of high surface area monoclinic WO_3 particles using organic ligands and emulsion based methods, *J. Mater. Chem.*, **12**, 983–989.

Matalkeh, M., Nasrallah, G. K., Shurrab, F. M., Al-Absi, E. S., Mohammed, W., Elzatahry, A. & Saoud, K. M. (2022) Visible light photocatalytic activity of Ag/WO_3 nanoparticles and its antibacterial activity under ambient light and in The dark, *Results Eng.*, **13**, 100313.

Matei, E., Rapa, M., Predescu, A. M., Țurcanu, A. A., Vidu, R., Predescu, C. & Orbeci, C. (2021) Valorization of agri-food wastes as sustainable eco-materials for wastewater treatment: current state and new perspectives, *Materials*, **14** (16). https://doi.org/ 10.3390/ma14164581.

Moja, M. M., Mapossa, A. B., Martin, E., Chirwa, N. & Tichapondwa, S. (2024) Photocatalytic degradation of 2,4-dichlorophenol using nanomaterials silver halide catalysts, *Environ. Sci. Pollut. Res.*, **31**, 11857–11872.

Nezamzadeh-Ejhieh, A. & Ghanbari-Mobarakeh, Z. (2015) Heterogeneous photodegradation of 2,4-dichlorophenol using FeO doped onto nano-particles of zeolite P, *J. Ind. Eng. Chem.*, **21**, 668–676.

Olaniran, A. O. & Igbinosa, E. O. (2011) Chlorophenols and other related derivatives of environmental concern: Properties, distribution and microbial degradation processes, *Chemosphere*, **83**, 1297–1306.

Ozkan Zayim, E., Liu, P., Lee, S. H., Edwin Tracy, C., Turner, J. A., Pitts, J. R. & Deb, S. K. (2003) 'Mesoporous sol–gel WO_3 thin films via poly (styrene-co-allyl-alcohol) copolymer templates', *Solid State Ion.*, **165**, 65–72.

Pokhrel, S., Simion, C., Teodorescu, V., Barsan, N. & Weimar, U. (2009) Synthesis, mechanism, and gas-sensing application of surfactant tailored tungsten oxide nanostructures, *Adv. Funct. Mater.*, **19**, 1767–1774.

Ranjit, P. J. D., Palanivelu, K. & Lee, C. S. (2008) 'Degradation of 2, 4,-dichlorophenol in aqueous solution by sono-Fenton method', *J. Chem. Eng.*, **25** (1), 112–117.

Ren, L., Zhang, J., Li, Y. & Zhang, C. L. (2011) Preparation and evaluation of cattail fiber-based activated carbon for 2,4-dichlorophenol and 2,4,6-trichlorophenol removal, *Chem. Eng. J.*, **168**, 553–561.

Saxena, G., Chandra, R. & Bharagava, R. N., (2016) Environmental pollution, toxicity profile and treatment approaches for tannery wastewater and its chemical pollutants. In: de Voogt, P. (ed.) *Reviews of Environmental Contamination and Toxicology*, Cham: Springer, pp. 240. https://doi.org/10.1007/398_2015_5009.

Shakoor, I., Jabeen, U., Ahmad, I., Riaz, S., Tayyab, M., Syed, A., Bahkali, A. H., Riaz, M., Zairov, R. R. & Zafar, M. N. (2024) Zns and Fe-doped ZnS photocatalysts for improved visible light driven photocatalytic degradation of methylene blue, *Inorganica Chim. Acta*, **560**, 121837.

Shankar, S. S., Rai, A., Ahmad, A. & Sastry, M. (2004) Rapid synthesis of Au, Ag and bimetallic Au core-Ag shell nanoparticles using neem (*Azadirachta indica*) leaf broth, *J. Colloid Interface Sci.*, **275**, 496–502.

Sherlya, E. D., Judith Vijaya, J., Clament Sagaya Selvama, N. & John Kennedy, L. (2014) Microwave assisted combustion synthesis of coupled ZnO–ZrO_2 nanoparticles and their role in the photocatalytic degradation of 2,4-dichlorophenol, *Ceram. Int.*, **40**, 5681–5691.

So, C. M., Cheng, M. Y., Yu, J. C. & Wong, P. K. (2002) Degradation of azo dye procion Red MX-5B by photocatalytic oxidation, *Chemosphere*, **46**, 905–912.

Su, R., Tiruvalam, R., He, Q., Dimitratos, N., Kesavan, L., Hammond, C., Lopez-Sanchez, J. A., Bechstein, R., Kiely, C. J. & Hutchings, G. J. (2012) Promotion of phenol photodecomposition over TiO_2 using Au, Pd, and Au–Pd nanoparticles, *ACS Nano*, **6**, 6284–6292.

Sun, M., Xu, N., Cao, Y. W., Yao, J. N. & Wang, E. G. (2000) Nanocrystalline tungsten oxide thin film: preparation, microstructure, and photochromic behavior, *J. Mater. Res.*, **15**, 927–933.

Tayyab, M., Kulsoom, U. E., Liu, Y., Mansoor, S., Khan, M., Akmal, Z., Mushtaq, A., Arif, M., Shamriaz, U., Zhou, L., Lei, J. & Zhang, J. (2024) Visible light-driven photocatalytic H_2 evolution and dye degradation by electrostatic self-assembly of CdS nanowires on nb_2c MXene, *Int. J. Hydrog. Energy*, **51**, 1400–1413.

Trombino, S., Cassano, R., Procopio, D., Di Gioia, M. L. & Barone, E. (2021) Valorization of tomato waste as a source of carotenoids, *Molecules*, **26** (16). https://doi.org/ 10.3390/molecules26165062.

Vignesh, K., Suganthi, A., Rajarajan, M. & Sara, S. A. (2012) Photocatalytic activity of AgI sensitized ZnO nanoparticles under visible light irradiation, *Powder Technol.*, **224** (331).

Wang, Y. Q., Gu, B. & Xu, W. L. (2009) Electro-catalytic degradation of phenol on several metal-oxide anodes, *J. Hazard. Mater.*, **162**, 1159–1164.

Wang, P. Q., Bai, Y., YaLuo, P. & Liu, J. Y. (2013) 'Assembly of ZIF nanostructures around free Pt nanoparticles: Efficient size-selective catalysts for hydrogenation of alkenes under mild conditions', *Catal. Commun.*, **38**, 75–82.

Zhang, Z., Shen, Q. H., Cissoko, N., Wo, J. & Xu, X. (2010) Catalytic dechlorination of 2,4-dichlorophenol by Pd/Fe bimetallic nanoparticles in the presence of humicacid, *J. Hazard. Mater.*, **182**, 252–258.

Zhao, Z. & Miyauchi, M. (2008) Nanoporous-walled tungsten oxide nanotubes as highly active visible-light-driven photocatalysts, *Angew. Chem. Int. Ed.*, **47**, 7051–7055.

Zhao, C., Pelaez, M., Dionysiou, D. D., Pillai, S. C., Byrne, J. A. & O'Shea, K. E. (2014) UV and visible light activated TiO_2 photocatalysis of 6-hydroxymethyl uracil, a model compound for the potent cyanotoxincylindrospermopsin, *Catal. Today.*, **224**, 70–76.

Zheng, H., Ou, J., Strano, M., Kaner, R., Mitchell, A. & Kalantarzadeh, K. (2011) Nanostructured tungsten oxide – Properties synthesis and applications, *Adv. Funct. Mater.*, **21**, 2175–2196.

Zhou, T., Li, Y. Z. & Lim, T. T. (2010) *Sep. Purif. Technol.*, **76**, 206–214.

Zhou, J., Yu, X., Ding, C., Wang, Z., Zhou, Q., Pao, H. & Cai, W. (2011) Optimization of phenol degradation by *Candida tropicalis* Z-04 using Plackett–Burman design and response surface methodology, *J. Environ. Sci.*, **23**, 22–30.

First received 7 August 2024; accepted in revised form 22 October 2024. Available online 6 November 2024